Condensed Matter Physics, 2026, Vol. 29, No. 3, 33502: 1–17
DOI: 10.5488/CMP.29.33502
ISSN: 1607-324X https://cmpj2.icmp.lviv.ua

CONDENSED MATTER PHYSICS

Molecular dynamics simulations of DMSO–MeOH liquid mixtures. Effects of force fields on mixing properties

M. Cruz-Sánchez [1], O. Pizio [2] *

[1] Departamento de Química, Universidad Autónoma Metropolitana-Iztapalapa, Av. San Rafael Atlixco 186, Col. Vicentina, 09340 CDMX, México

[2] Instituto de Química, Universidad Nacional Autónoma de México, Circuito Exterior, 04510 Cd. Mx., México

Received 29 June 2026; revised 28 July 2026; accepted 31 July 2026; published 28 September 2026

We explore composition dependence of the principal properties of liquid dimethylsulfoxide (DMSO)-methanol (MeOH) liquid mixtures by using molecular dynamics computer simulations. A set of non-polarizable semi-flexible models for the DMSO molecule combined with methanol models is investigated. Composition trends of density, excess mixing volume and excess mixing enthalpy are evaluated. Besides, we study the composition dependence of self-diffusion of species and shear viscosity of the static dielectric constant and the surface tension. Certain aspects of the microscopic structure are analyzed in terms of radial distribution functions and of the average number of hydrogen-bonded molecules. The quality of several combinations of the models is illustrated and critically evaluated by comparisons with experimental data.

Key words: *molecular dynamics, methanol, dimethylsulfoxide, density, dielectric constant, surface tension, self-diffusion coefficients, shear viscosity*

1. Introduction

There have been many experimental and computer simulation reports concerning measurements and interpretation of properties of binary mixtures involving dimethylsulfoxide as one of the components. This research was motivated by the practical importance of pure DMSO as a solvent in chemistry and chemical engineering [1–3]. Moreover, liquid mixtures of dimethylsulfoxide (DMSO) and water are used in several biological applications, the cryoprotection being just one of the examples [4–7]. Ionic solutes in water–DMSO mixed solvents have been studied for diverse practical objectives as well [8–10]. As discussed in [11] for example, the experimental knowledge and understanding of the microscopic structure and dynamic properties of these systems follows mainly from the application of calorimetry, neutron scattering, nuclear magnetic resonance, dielectric relaxation and vibrational spectroscopy methods. Hence, a set of experimental data for this class of mixtures is quite comprehensive.

Less attention has been paid to mixtures of DMSO (and its analogues, like diethylsulfoxide) with non-aqueous solvents. These systems, however, are of both practical importance and academic interest as documented in several publications, see e.g., [12–18]. Finally, multi-component mixtures that involve salts and/or room temperature ionic liquids besides DMSO and/or other species (e.g., water), were investigated recently [19–24].

In order to interpret the experimental results in detail and to get ampler insights with predictive power, one is forced to resort to computer simulation methodology. Usual strategy of computer simulations is to choose a model of each species, i.e. the intra-molecular structure at a certain level of sophistication,

*Corresponding author: oapizio@gmail.com.

and assume the inter-molecular interactions. Commonly, the combination rules are used for the cross interaction between species.

Most frequently used and quite well tested non-polarizable models for monohydric alcohols are the ones at a united atom and all-atom levels, see e.g., [25–29]. Similar united atom level models for DMSO species were proposed in the original publications (cited below) and reviewed in detail in [30, 31]. A more sophisticated force fields for DMSO were investigated as well [32, 33]. Namely, a flexible all-atom model of DMSO was developed in [32] and tested in a few aspects for DMSO-water (TIP3P) mixtures. On the other hand, Bachmann and van Gunsteren, [33], proposed computationally demanding, polarizable model for DMSO and combined it with polarizable water model. Extensive tests for DMSO–water systems were performed and suggested that simpler, non-polarizable models with successful parametrization preserve competitive level.

Adequacy of the computer simulation predictions for a given model should be tested by comparison with experimental data. In general terms, computer simulations permit to interpret observables at microscopic level with molecular level details. Besides, a wider set of properties, in comparison with experimental results, can be obtained with a reasonable degree of confidence.

In the design of alcohol models at a united atom level, e.g., the UAMI-EW set of models from [27], the target properties for fitting of the force field are the density, the surface tension and the dielectric constant. Throughout this report we use abbreviation UAMI rather than UAMI-EW for the sake of brevity. This kind of parametrization was quite successful for a single-component monohydric alcohols on temperature and pressure, and for their mixtures with water at a room temperature and ambient pressure [27, 34, 35]. However, our recent study elucidated deficiencies of this type of force field upon its application for mixtures of different alcohols [36]. Similar problem has been encountered while using TraPPE force field for mixtures of primary and secondary alcohols [37].

Concerning the DMSO modelling at a united atom level, one should note that most common targets include solely the liquid density and the vaporization enthalpy, see e.g., [38]. Certain adjustments of parameters to yield various properties were used in some cases for the sake of better performance as discussed in [30] for example. Still, the principal attention of many studies was to apply the pure DMSO united atom models and explore the properties of DMSO–water mixtures.

In spite of availability of experimental data for various properties of DMSO–alcohol mixtures, we have found the only previous investigation of binary DMSO–methanol system by using molecular dynamics simulation in [39]. These authors used the OPLS united atom type models for both species, MeOH and DMSO, respectively. Principal findings of this work have been restricted to the exploration of composition changes of microscopic structure, self-diffusion coefficients and molecular reorientation times without comprehensive comparisons with experimental predictions.

Having this in mind, the principal objective of the present work is to investigate, as comprehensively as possible, the mixing properties of methanol and DMSO by using a wide set of united-atom models for both species and molecular dynamics methodology. We would like to critically evaluate the results of simulations versus experimental data in order to proceed to a more sophisticated modelling in future work and to attempt an extension for a more complex alcohol species.

2. Models and simulation details

In this work we restrict our attention to a set of DMSO united atom type, non-polarizable models with four sites, O, S, CH_3 (methyl group consisting of carbon and hydrogen atoms is replaced by a single CH_3 interaction site located on the methyl carbon atom). The CH_3 group is abbreviated as C in what follows. Within this modelling, the interaction potential between all atoms and/or groups is assumed as a sum of Lennard-Jones (LJ) and Coulomb terms. Similarly, the united atom type modelling is considered for methanol species. For this subsystem we restrict our attention to the UAMI model and TraPPE force field. Both of them were previously tested on several occasions to reproduce properties of monohydric alcohols–water mixtures.

A comprehensive description of the parameters of models of this type is given in tables 1–3 below. The nomenclature of models is taken from the original publications indicated in the first column of table 1.

Table 1. Parameters of Lennard-Jones site-site interaction for DMSO models. The energies are given in kJ/mol whereas the diameters are in Å.

Model	ε_{OO}	σ_{OO}	ε_{SS}	σ_{SS}	ε_{CC}	σ_{CC}
P2 [40]	0.2992	2.80	0.9974	3.40	1.230	3.80
OPLS [41]	1.171	2.93	1.652	3.56	0.669	3.81
VB [42]	0.276	2.94	0.842	3.56	0.669	3.60
VLL [43]	0.591	2.92	1.398	3.66	0.957	3.76
GOVG [38]	1.7154	2.63	1.2972	3.56	0.86718	3.748
Bordat et al. [44]	1.7154	2.63	1.297	3.56	0.9414	3.739

Similar information and nomenclature for DMSO models, the reader can find in table 1 of [30], in table 1 of [31], and in [38, 43]. In our table, some misprints from table 1 of [31] were corrected. The most important misprint in the original paper [43] was the value for ε_{CC}, which was discovered first by Geerke et al. [38]. In addition, we take the original value for σ_{CC} from [43], in contrast to [31].

Table 2. Charges of sites for the united atom DMSO models (in units of elementary charge).

Model	q_O	q_S	q_C
P2, OPLS, VB, VLL	−0.459	0.139	0.16
GOVG	−0.44753	0.12753	0.16
Bordat	−0.43674	0.11674	0.16

Finally, the parameters describing intramolecular structure of DMSO molecule are: l_{OS} = 1.53 Å and l_{SC} = 1.80 Å (P2, OPLS, VLL models); l_{OS} = 1.53 Å and l_{SC} = 1.95 Å (Bordat et al. model); l_{OS} = 1.53 Å and l_{SC} = 1.93799 Å (GOVG model) and l_{OS} = 1.496 Å and l_{SC} = 1.80 Å (VB model), respectively. The angles are as follows O-S-C = 106.75°, C-S-C = 97.4° (for P2, OPLS, VLL, GOVG and Bordat et al.); 107.2°, and 99.2° (for VB model), respectively. In addition, the improper dihedral S-C-O-C is included into the DMSO models according to [45]. This issue was discussed in our previous studies of water–DMSO mixtures [46, 47].

Table 3. Parameters of Lennard-Jones site-site interactions for methanol models. The C-O-H angle is 108.5°; l_{OH} = 0.945 Å, l_{CO} = 1.43 Å.

Model	ε_{OO}	σ_{OO}	ε_{CC}	σ_{CC}	q_O	q_C	q_H
TraPPE	0.773245	3.02	0.814817	3.75	−0.700	0.265	0.435
UAMI	0.68208	3.1808	0.71877	3.6783	−0.77147	0.29252	0.47895

Molecular dynamics computer simulations of DMSO–methanol mixtures have been performed in the isothermal-isobaric (NPT) ensemble at atmospheric pressure 1 bar and at temperature 298.15 K. We used GROMACS package [48] version 5.1.2. The simulation box in each run was cubic, the total number of molecules is fixed at 3000. Composition of the mixture is described by the mole fraction of DMSO molecules, $X_D = N_{DMSO}/(N_{DMSO} + N_{MeOH})$. As common, periodic boundary conditions were used. Temperature and pressure control was provided by the V-rescale thermostat and Parrinello-Rahman barostat with $\tau_T = 0.5$ ps and $\tau_P = 2.0$ ps, the timestep was 0.002 ps. The value of $5.25 \cdot 10^{-5}$ bar^{-1} was used for the compressibility of mixtures. Lorentz-Berthelot combination rules (CR2 in Gromacs nomenclature) were used to determine cross parameters for the relevant potential well depths and diameters for all models. The models for MeOH, UAMI and TraPPE, imply application of CR2 rules. Moreover, the P2, VLL, GOVG and Bordat et al. models for DMSO were studied by using the CR2 rules as well. Solely, the OPLS modelling requires the application of CR3 rules. In summary, in the present study we restrict only to the CR2 procedure for all models, in close similarity to the study of the entire set of DMSO–water models (with CR2 rules) in [31].

The non-bonded interactions were cut-off at 1.1 nm, whereas the long-range electrostatic interactions were handled by the particle mesh Ewald method implemented in the GROMACS software package (fourth order, Fourier spacing equal to 0.12) with the precision 10^{-5}. The van der Waals correction terms to the energy and pressure were applied. In order to maintain the geometry of molecules, the LINCS algorithm was used.

After preprocessing and equilibration, several consecutive simulation runs with the starting configuration being the last configuration from the previous run, were performed to obtain trajectories for the data analysis. The results for each property were obtained by averaging over pieces (20–30 ns) of the entire trajectories not less than 150 ns. Additional details concerning calculations of the surface tension and shear viscosity are given in the respective sections below.

3. Results and discussion

Nikam et al. [49] reported experimental results for the composition dependence of density and viscosity of DMSO-alkanols (methanol, ethanol, propanol, etc.) mixtures at 298.15 K and 303.15 K. Besides, these authors provided the excess mixing volume and the excess viscosity (in figures 2 and 3 of [49]). Previous simulation work, [39], does not report these properties.

3.1. Density and molar volume of DMSO–MeOH mixtures on composition

We use experimental data of Nikam et al. at a room temperature $T = 298.15$ K, and atmospheric pressure [49]. In the first figure, figure 1, we show the dependence of density on composition for a single DMSO model, P2 from [40], combined with either UAMI [27] or TraPPE [26] MeOH models. The P2 model for DMSO was chosen quite arbitrarily, mainly to keep track of our previous studies of DMSO–water mixtures, [46, 47].

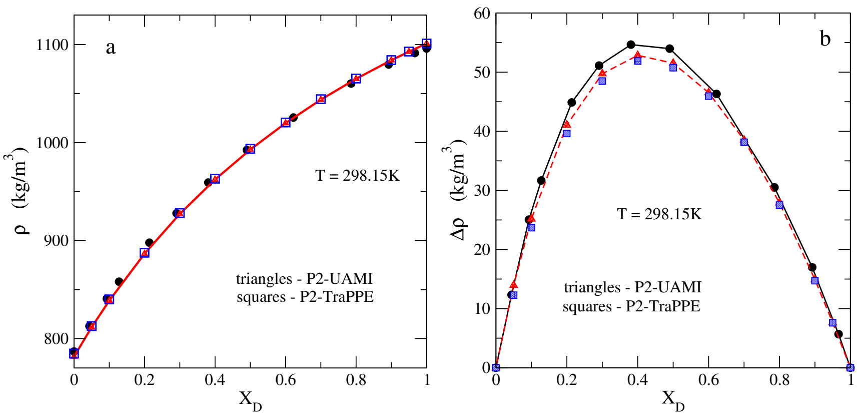

Figure 1. (Colour online) Panels a and b: The dependence of DMSO–MeOH density (panel a) and of the excess density (panel b) on mole fraction of DMSO, X_D. The simulation results are for P2–UAMI (red) and for P2–TraPPE (blue) united atom models. The experimental data (black circles) are from [49]. The nomenclature of symbols is given in both panels of the figure. All the results in the figures throughout this work refer to $T = 298.15$ K and $P = 1$ bar, unless specified.

Previously, it was shown that the principal improvement achieved by the UAMI methanol model, in comparison to the TraPPE one, for pure methanol, is in a much better dielectric constant of the former, whereas other properties, e.g., density are of the same quality. Similar conclusion, concerning $\rho(X_D)$ for DMSO–MeOH mixtures, is illustrated in figure 1a. The simulation data accurately reproduce experimental behavior of density on composition. Moreover, both methanol models, if combined with the P2 DMSO force field, yield correct and quite accurate description of the deviation of density of the mixture from ideality ($\Delta\rho = \rho - X_\mathrm{D}\rho_D - (1 - X_\mathrm{D})\rho_M$) in the entire composition range, figure 1b.

In the following figure, figure 2, we consider a single methanol model, UAMI, and explore the composition dependence of density for various DMSO models described in table 1. It can be seen that the VLL–UAMI model yields most accurate predictions. On the other hand, the VB–UAMI model is the least accurate, it leads to a qualitatively correct predictions but deviates from experimental points in the interval of intermediate composition.

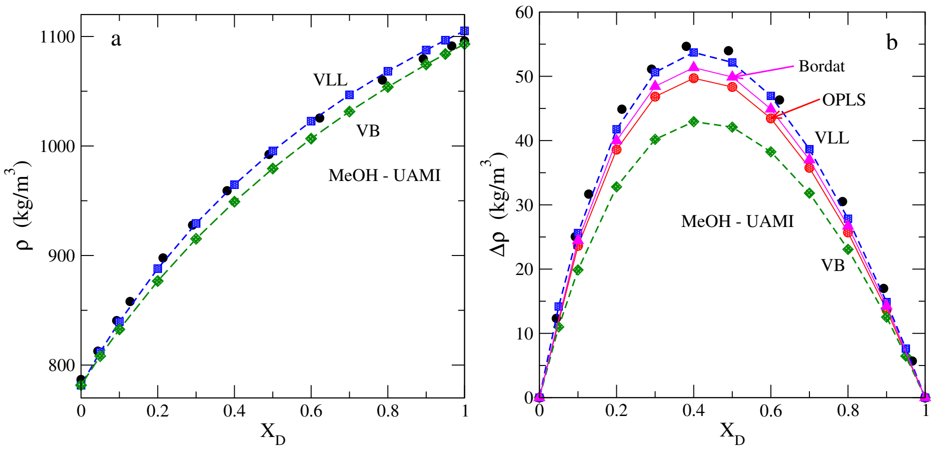

Figure 2. (Colour online) Panels a and b: The dependence of DMSO–MeOH density (panel a) and of the excess density (panel b) on DMSO mole fraction, X_D. The experimental data (black circles) are from [49]. The nomenclature of colors and symbols is given in both panels of the figure.

Frequently, for chemical engineering purposes, the experimental data are reported in terms of the excess mixing volume, ΔV_{mix}. It is defined by the same expression as $\Delta\rho$ above, just for molar volumes rather than the densities, see e.g., equation (2) of [50].

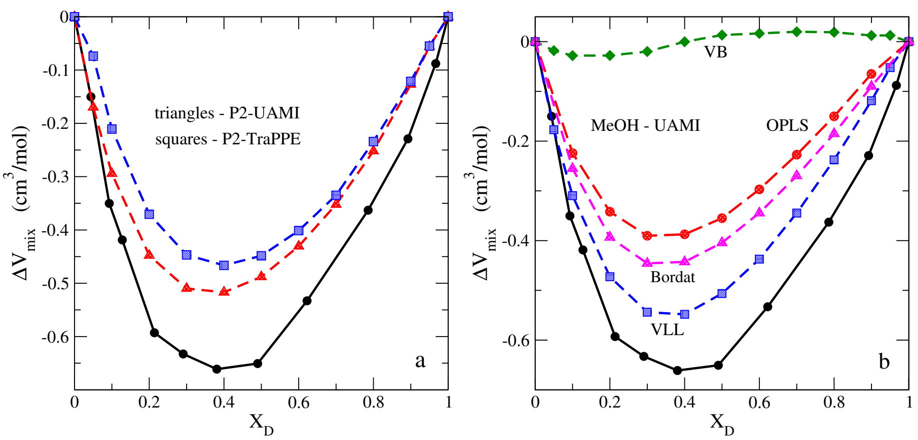

Figure 3. (Colour online) Panels a and b: The dependence of DMSO–MeOH excess molar volume on composition. The simulation results are for the P2–UAMI and for P2–TraPPE united atom model in panel a. In panel b, the simulation data are for OPLS–UAMI, VLL–UAMI, VB–UAMI and Bordat–UAMI united atom models. The experimental data (black circles) are from [49] in both panels. The nomenclature of colors and symbols is given in the figures.

This representation yields enhanced insight into the accuracy of $\rho(X_D)$ curves. Our simulation data for different models and comparison with experimental results are shown in figure 3. The curves in panel a of this figure provide insight of the effect coming from changes of MeOH model whereas panel b illustrates the effect of changes of ΔV_{mix} for different DMSO models. From panel a of this figure we conclude that both MeOH models combined with P2 DMSO provide reasonable results for the excess mixing volume. The UAMI model is slightly better than the TraPPE one for this specific property. Panel b of figure 3 illustrates quality of the curves for $\Delta V_{\text{mix}}(X_{\text{D}})$ upon changes of the DMSO models for a given MeOH force field. These results confirm that the VLL–UAMI model yields quite accurate predictions. By contrast, the VB–UAMI model is not satisfactory for the excess mixing volume. This behavior is due to the differences in the choice of parameters of Lennard-Jones interaction as well as due to the details of intramolecular structure, because the charge distribution for VLL and VB models is the same. In summary, one can use various united atom models for DMSO–MeOH mixtures to describe geometric aspects of mixing (in terms of excess density and mixing volume) accurately. Additional test of different models involves calculation of the excess mixing enthalpy. We refer to this property as to the descriptor of the energetic aspects of mixing.

3.2. Energetic aspects of mixing

In figure 4, we present the simulation results for excess mixing enthalpy and make comparison with experimental data. It is a very sensitive property, to capture it accurately presents a real challenge for the force field.

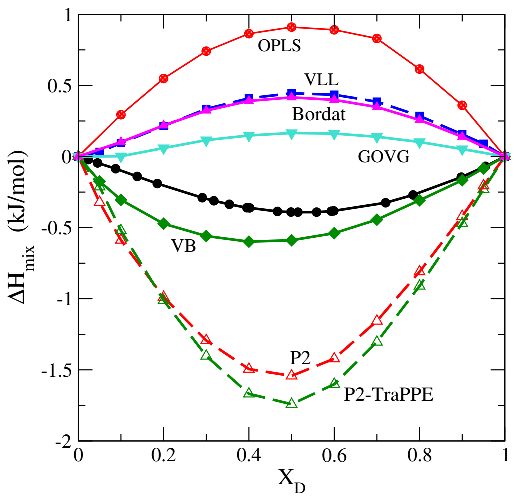

Figure 4. (Colour online) The dependence of the excess mixing enthalpy on composition for various models of DMSO–MeOH mixtures (indicated in the figure). The experimental data (black circles) are from [51].

We observe that the models of the present study are not entirely satisfactory. Some of them predict endothermic heat of mixing in contrast to exothermic mixing from the experimental data. The best agreement with experimental results is observed from the VB–UAMI model. The worst behavior, with correct sign but in terms of absolute values, comes from P2–UAMI and P2–TraPPE models. Smaller deviation from the experimental data, but with incorrect sign, is obtained, if the VLL, Bordat, GOVG DMSO models are combined with UAMI force field for MeOH. This behavior is slightly disappointing. Actually, it should be attributed to inaccurate description of the energetics of cross interaction between species or more precisely to the description of energetic balance between interaction of similar and dissimilar species.

In order to get a deeper insight into these trends, we have undertaken calculations of the structural aspects of mixing in terms of pair distribution functions and of evolution of the number of hydrogen bonds in the system upon changes of composition.

3.3. Structural aspects of mixing

To begin with, we present the pair distribution functions of oxygens belonging to methanol and DMSO at methanol-rich ($X_D = 0.05$), DMSO-rich ($X_D = 0.95$) and intermediate composition ($X_D = 0.5$) of the mixture in the following figures. Two models, P2 and VLL, for DMSO have been taken because they yield a rather different behavior of $\Delta H_{mix}(X_D)$ in figure 4. Thus, our principal issue is to elucidate the differences in the evolution of microscopic structure upon changes of DMSO content in the model mixtures.

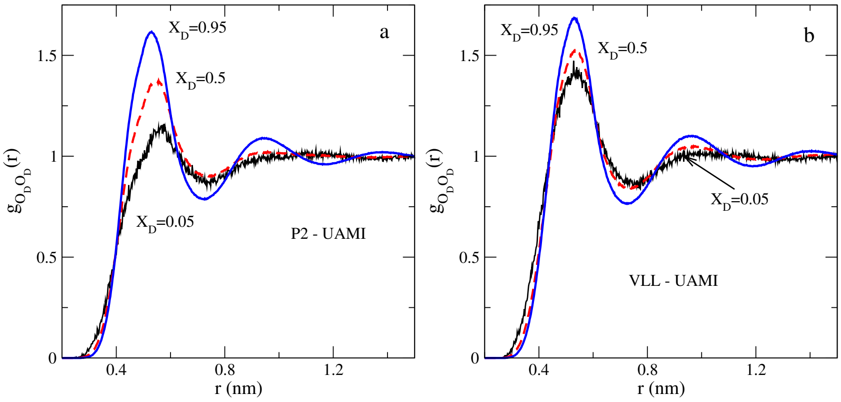

Figure 5. (Colour online) Evolution of the distribution of the DMSO oxygens, O_DO_D, on the mole fraction of DMSO species in the mixture.

Concerning the O_D-O_D distribution, we observe that the development of the short-range structure is qualitatively similar in the P2–UAMI and VLL–UAMI models, figure 5. Certain quantitative difference can be seen in the rate of growth of the first maximum of the distribution function when X_D increases from 0.05 to 0.5, however. Subtle differences in the changes of structure might develop due to the differences of parameters of Lennard-Jones direct interaction and dipole-dipole intermolecular potential, besides correlation via methanol species.

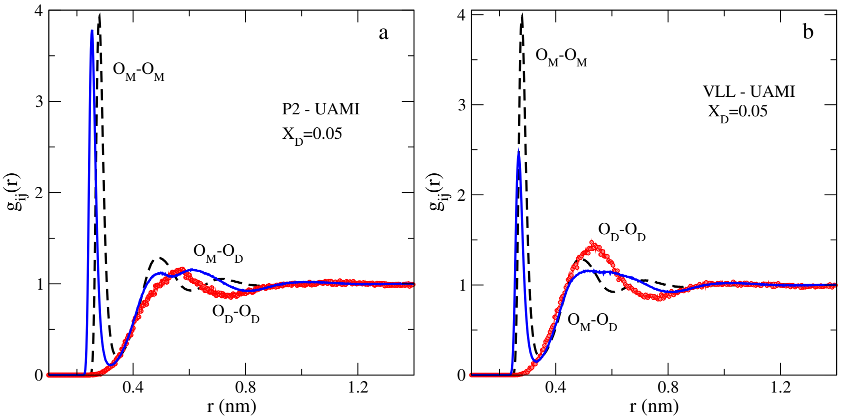

Figure 6. (Colour online) Pair distribution functions of oxygens belonging to methanol species, O_MO_M (black dashed lines), cross, O_MO_D (blue solid lines), and of oxygens of DMSO molecules O_DO_D (red lines) at $X_D = 0.05$. Panel a refers to P2–UAMI model whereas panel b is for VLL–UAMI model. The same nomenclature of colors is used in figures 6–8.

Evolution of the cross pair distribution function between oxygens belonging to different species, O_MO_D, exhibit similar trends for both models in question as well, figures 6–8. Specifically, the height of the first maximum of this function increases with increasing X_D from 0.05 up to 0.5, figure 6 and 7. Next, it saturates and even decreases slightly for the P2–UAMI models, whereas for the VLL–UAMI one, the first maximum keeps growing, cf. figure 6 and figure 7.

The principal difference in changes of the microscopic structure of two models can be observed in terms of $O_M O_M$ distribution, figures 6–8. At a low DMSO concentration, i.e., in methanol-rich mixtures, two models confirm very similar and strong correlation between MeOH molecules, figure 6. Apparently, the DMSO molecules show stronger affinity to methanol particles in the P2–UAMI model compared to the VLL–UAMI one, as it follows from the first maximum of $O_M O_D$ distribution, figure 6.

However, the height of the first maximum of $O_M O_M$ distribution gradually decreases upon increasing X_D within the P2–UAMI model, cf. figure 7a and figure 8a. By contrast, this maximum gradually grows with increasing X_D within the VLL–UAMI model, cf. figure 7b and figure 8b. This behavior is accompanied by increasing strength of affinity of O_M and O_D atoms, as it follows from changes of $O_M O_D$ distribution. Nevertheless, the magnitude of correlations between dissimilar species, O_M and O_D, is quite different for two models, witnessed by the height of the first maximum of $O_M O_D$ distribution in panels a and b of these three figures, figures 6–8.

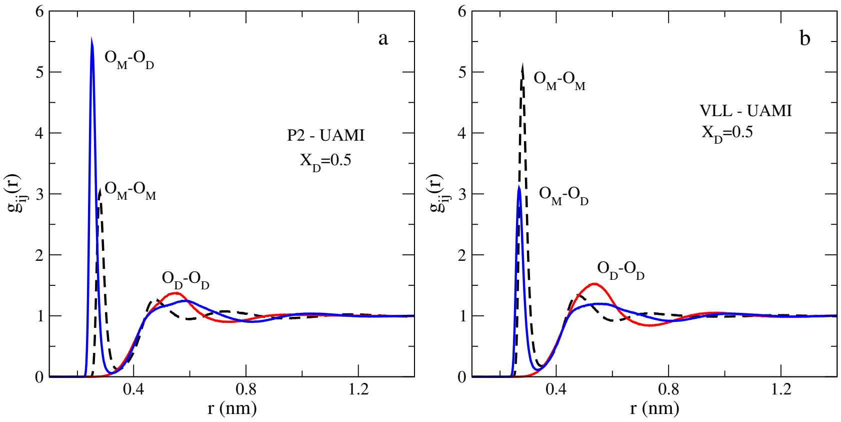

Figure 7. (Colour online) The same as in figure 6 for the mixture with equimolar composition ($X_D = 0.5$).

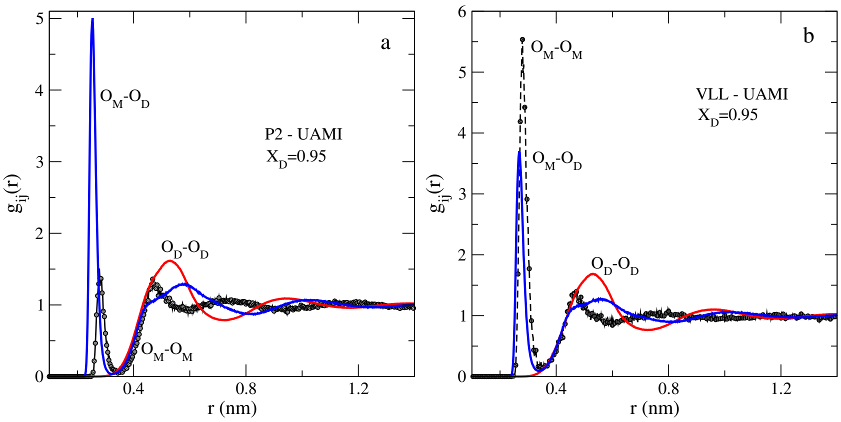

Figure 8. (Colour online) The same as in figure 6 and figure 7 but for DMSO-rich mixture with $X_D = 0.95$.

It is difficult to extract a more detailed information concerning changes of the microscopic structure and interpret predictions from the pair distribution functions at united atom level modelling without additional assumptions. One needs to assume the all-atom models to perform comparisons with the experimentally reachable structure factors. We refer to [34, 52, 53] for detailed discussion of this issue. Unfortunately, we are not aware of the experimental measurements of the structure factors either from X-ray of neutron diffraction techniques.

Additional insights into the structure of the mixtures in question follow from the analysis of hydrogen bonding. The average number of hydrogen bonds per methanol molecule was obtained using the gmx hbond utility with default options (it implies geometric criterion for H-bonding) of the GROMACS software. The reader can find a more detailed description of the criteria and methods used to characterize hydrogen bonding effects in [54–56]. Our results are shown in figure 9.

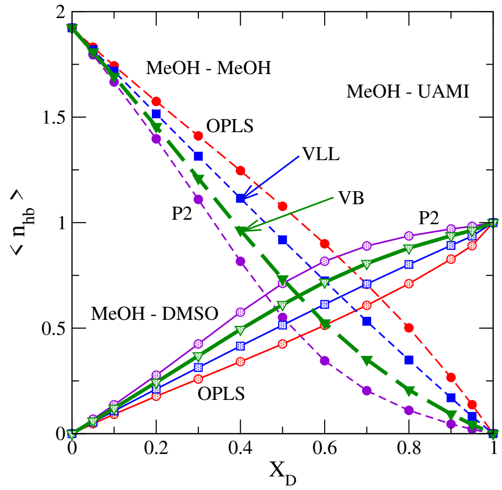

Figure 9. (Colour online) The dependence of the average number of hydrogen bonds on composition for various models of DMSO–MeOH mixtures (indicated in the figure). Solid lines describe cross hydrogen bonding, i.e., between DMSO and MeOH molecules, whereas the dashed lines illustrate bonding between methanol species.

General trends of behavior of the number of molecules participating in hydrogen bonds on the DMSO mole fraction are quite similar from model to model. Namely, the average number of methanol molecules that form H-bonds between themselves, $\langle n_{hb} \rangle_{\rm MM}$, decreases with increasing the DMSO content in the mixture. On the other hand, the number of cross hydrogen bonds between methanol and DMSO molecules, $\langle n_{hb} \rangle_{\rm MD}$, increases with increasing $X_{\rm D}$. At a low DMSO content, the methanol molecules form two H-bonds between themselves, proving the formation of a certain number of methanol chains in the system under such conditions. On the other hand, in the DMSO-rich mixtures, the methanol molecules form one bond on average with DMSO species while MeOH–MeOH bonds are improbable.

Interestingly, the balance between the numbers describing bonding between similar and dissimilar species is different for different models. To keep track with the performance of the models in question for the excess mixing enthalpy, we would like to comment the bonding in P2- UAMI and VLL–UAMI models. In the former case, P2–UAMI, the $\langle n_{hb} \rangle_{\rm MM}$ drops most rapidly with increasing $X_{\rm D}$, compared to other models, e.g., the VLL–UAMI. On the other hand, the $\langle n_{hb} \rangle_{\rm MD}$ increases most fast upon $X_{\rm D}$ within P2–UAMI model, compared to other models, figure 9. However, at a high DMSO content, one can observe trends for $\langle n_{hb} \rangle_{\rm MD}$ saturation, in contrast to other models under study. The most pronounced deviation (of opposite sign) of the excess mixing enthalpy for the models of our attention, P2 and VLL, from experimental results occurs at intermediate composition, $X_{\rm D} \approx 0.5$, cf. figure 4. At such composition, the average number of cross bonds, $\langle n_{hb} \rangle_{\rm MD}$, is larger than the $\langle n_{hb} \rangle_{\rm MM}$ for P2–UAMI model, figure 9. By contrast, we observe that $\langle n_{hb} \rangle_{\rm MD}$ is substantially lower than $\langle n_{hb} \rangle_{\rm MM}$ for VLL–UAMI model in this interval of intermediate composition. Indeed, the balance of bonding of species in the mixture is reflected in the model predictions of excess mixing enthalpy. As a finishing touch of this subsection, we would like to attract attention of the reader to the experimental findings concerned with the role of methyl groups in hydrogen bonding [57]. An all-atom modelling of methanol and DMSO is required to address the issues resulting from these experiments. A comparison of spectra obtained via auto-correlation functions at a different level of modelling, would provide a more detailed insight into hydrogen bonding for the mixture in question.

3.4. Static dielectric constant

Our next concern is the description of the behavior of static dielectric constant, ε, for DMSO–MeOH mixture on composition. It is calculated by using common routine. Namely, ε is obtained from the time-average of the fluctuations of the total dipole moment of the system [58],

$$\varepsilon = 1 + \frac{4\pi}{3k_{\mathrm{B}}TV}\left(\langle \mathbf{M}^2\rangle - \langle \mathbf{M}\rangle^2\right), \tag{3.1}$$

where k_{B} is the Boltzmann constant and V is the simulation cell volume. The simulation results for two MeOH models combined with P2 DMSO, and different DMSO models combined with UAMI methanol are shown in figure 10a and 10b, respectively.

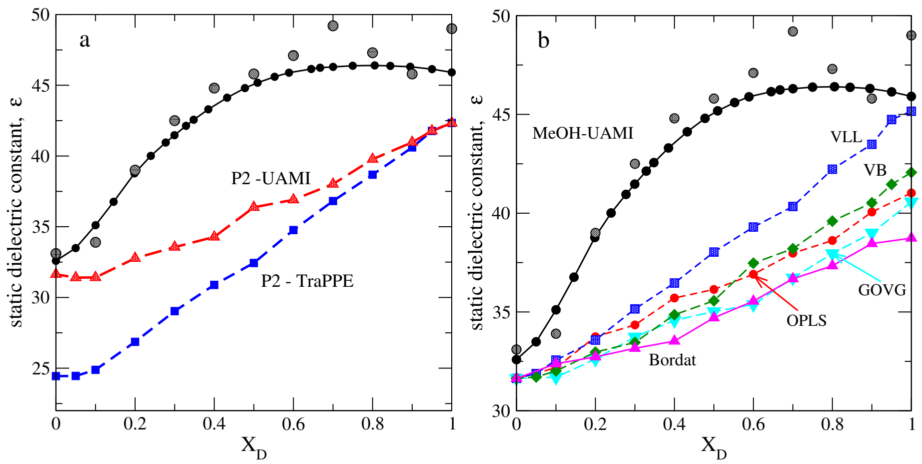

Figure 10. (Colour online) The dependence of the dielectric constant on composition for various models of DMSO–MeOH mixtures (indicated in the figure). The experimental data are from [59] (solid black circles) and [60] (dashed black circles).

We have already mentioned above that the principal improvement of the UAMI modelling in comparison with TraPPE is in a better description of the dielectric constant of pure alcohols. This is illustrated in figure 10a. The united atom P2 model for pure DMSO underestimates the dielectric constant, in comparison with the experimental result. The P2–UAMI model describes that the dielectric constant grows with increasing the DMSO content.

In some sense, the curves constructed from the simulation results for different DMSO models behave similarly, figure 10b. The dielectric constant grows from the value for pure methanol (around 30) to a higher value for the DMSO liquid. The VLL–UAMI leads to most reasonable values for DMSO-rich mixtures. However, the shape of the curves for $\varepsilon(X_{\mathrm{D}})$ resulting from experimental measurements and united atom type models is rather different. The simulation data of all these models do not correctly reproduce the deviation from ideality of $\varepsilon(X_{\mathrm{D}})$. This behavior due to modelling should be explored more in detail. Indeed, one needs to resort to all-atom models and to models that take into account polarizability in order to get certain answers. Particular attention should be paid to an appropriate description of cross hydrogen bonding between molecules belonging to different species. On pessimistic note, we are aware of the problem known already for DMSO–water mixtures [46, 47, 61]. It has not been solved so far even in the framework of one version of polarizable models [33].

3.5. Self-diffusion coefficients of species

Our results for the self-diffusion coefficients of methanol and DMSO species in the mixtures of different composition are shown in figure 11. They follow straightforwardly from the Einstein relation,

$$D_i = \frac{1}{6} \lim_{t\to\infty} \frac{\mathrm{d}}{\mathrm{d}t} |\mathbf{r}_i(\tau + t) - \mathbf{r}_i(\tau)|^2, \tag{3.2}$$

where τ denotes the time origin. Default settings of GROMACS were used for the separation of the time origins and for the fitting interval. We performed a couple of tests generating center of mass trajectories and used them to calculate the self-diffusion coeffients of species. However, the obtained results were very similar to the outputs from the GROMACS utility for the system under study. On the other hand, the self-diffusion coefficients can be obtained from the auto-correlation functions via Green-Kubo procedure. This method has not been used in the present work.

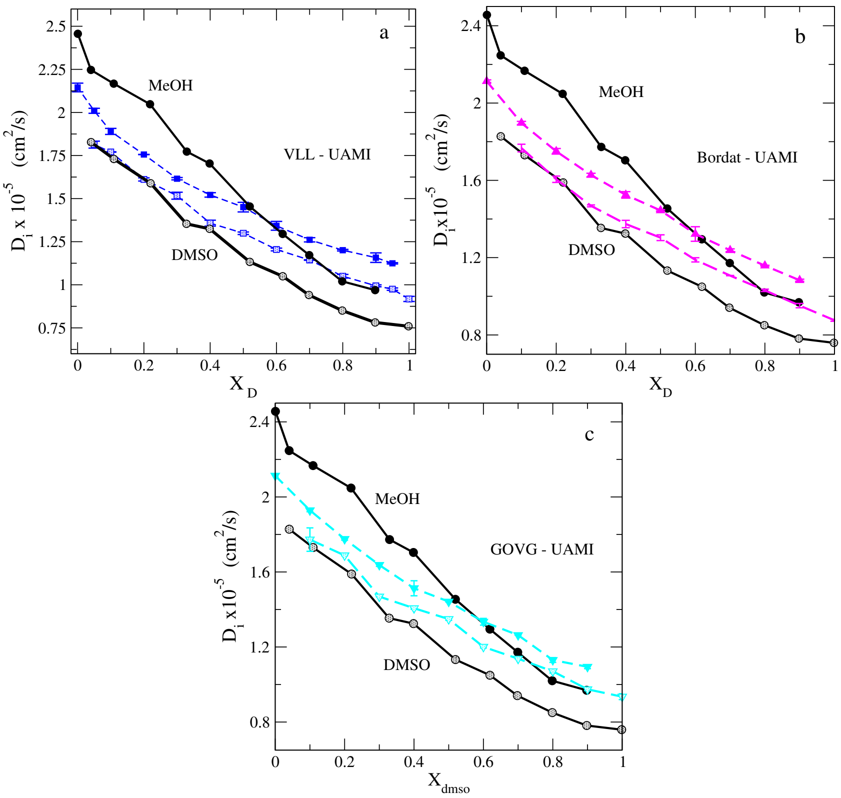

Figure 11. (Colour online) The dependence of the self-diffusion coefficients of species on composition for DMSO–MeOH mixtures with VLL–UAMI, Bordat–UAMI and GOVG–UAMI models, respectively. The nomenclature of colors for these models is like in figure 4. The experimental data (solid lines) are from [14]. The simulation data are shown by dashed lines. Solid symbols are for MeOH whereas hollow symbols are for DMSO.

Unfortunately, the experimental data of this property are scarce. According to the measurements given in [14], the D_{MeOH} is larger than D_{DMSO} in the entire composition range. The self-diffusion coefficients of both species monotonously decrease upon increasing the DMSO content in the mixture. Quality of the simulation results crucially depends on the adequate description for pure components. The best performance is provided by the VLL–UAMI, Bordat–UAMI and GOVG–UAMI models as seen in figure 11. Other two models suffer deficiencies yielding a crossover of the self-diffusion coefficients of methanol and DMSO species, in contrast to experimental data (see figure A.1 in the Appendix). We have not comprehensively explored the VB model for this property because it yields the self-diffusion coefficient for pure DMSO of the order of 2.5 (in close similarity to the model of Rao et al.

as documented in table 3 of [30]). In general, simulation results for the models illustrated in figure 11 are qualitatively correct. In quantitative terms, the models underestimate the methanol self-diffusion coefficient for methanol-rich mixtures and overestimate D_i for both species, methanol and DMSO, for DMSO-rich mixtures. There is enough room to improve the modelling of this property considering it as one of principal targets rather than mere output.

3.6. Shear viscosity of MeOH–DMSO mixtures

Now we present some results concerned with the dependence of viscosity of model mixtures under study on composition. We have chosen two models, VLL–UAMI and Bordat–UAMI, that describe self-diffusion coefficients most appropriately according to figure 11. Previously, the shear viscosity from simulations for DMSO–MeOH mixtures was not discussed, up to our best knowledge. Experimental data for shear viscosity of DMSO-alcohol mixtures are from [49, 62].

The shear viscosity, η, is calculated according to the common routine described in various publications. Namely,

$$\eta = \frac{V}{kT}\int_0^\infty \mathrm{d}t \left\langle P_{\alpha\beta}(0)P_{\alpha\beta}(t)\right\rangle , \qquad (3.3)$$

where, $\alpha, \beta = xy, xz$ and yz. In order to evaluate the shear viscosity from the integral above, we followed a procedure described in every detail by Gonzalez and Abascal, [63]. The statistical averages, given by points, follow from 3 - 6 independent simulations of the components of pressure tensor.

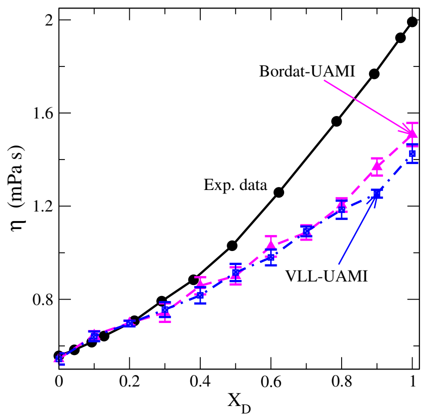

Figure 12. (Colour online) The dependence of shear viscosity on composition for DMSO–MeOH mixtures with VLL–UAMI (blue squares) and Bordat–UAMI (magenta triangles) models, respectively. The experimental data (black solid circles) are from [49].

Our simulation results are shown in figure 12. The line that joins the calculated points is provided for the sake of better visualization. The models in question describe shear viscosity reasonably well starting from methanol-rich mixtures up to intermediate composition in terms of X_D. For DMSO-rich mixtures, the models under study underestimate the values for shear viscosity in comparison with experimental data. This feature of DMSO models is known already from the studies of water-DMSO systems, see, e.g., [64]. The inaccuracy of the description of self-diffusion coefficients of species for methanol-rich mixtures does not influence the accuracy of results for shear viscosity. By contrast, overestimation of the self-diffusion coefficients of both species (M and D) for DMSO-rich mixtures, cf. figure 11, results in the underestimation of shear viscosity in this interval of composition.

3.7. Surface tension of DMSO-MeOH mixtures on composition

Our final remarks concern the behavior of the surface tension of DMSO-MeOH mixtures. The surface tension calculations at each composition have been performed by taking the final configuration of particles from the isobaric run. Next, the box edge along z-axis was extended by a factor of 3, generating a rectangular box with liquid slab and two liquid-mixture-vacuum interfaces in the $x-y$ plane, in close similarity to the procedure applied in [65]. The total number of molecules is sufficient to yield an area of the $x-y$ face of the liquid slab sufficiently big. The elongation of the liquid slab along z-axis is satisfactory as well. The effect of cutoff distance in the account of inter-particle interactions has been discussed in detail in [66]. Taking into account this analysis, in our calculations we used the cutoff distance equal to 2.2 nm, i.e., twice larger than for the bulk simulations.

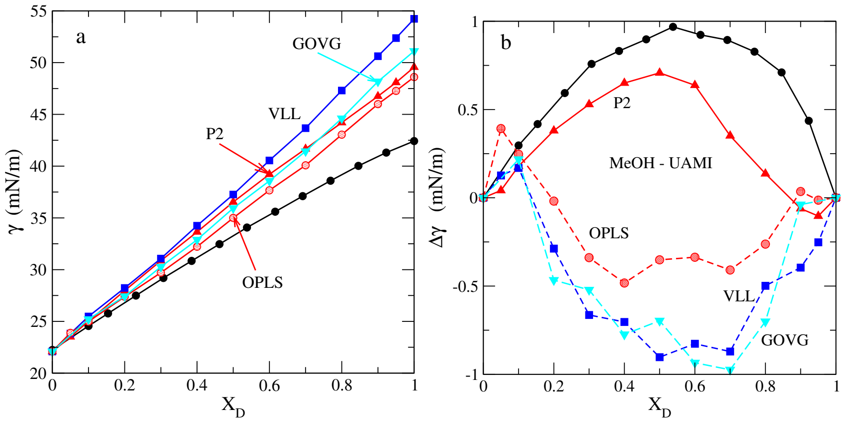

Figure 13. (Colour online) The dependence of the surface tension on composition (panel a) and of the excess surface tension (panel b) for DMSO–MeOH mixtures with UAMI methanol and various DMSO models. The experimental data are from [67].

The executable file has been modified by deleting the fixed pressure condition while preserving the V-rescale thermostatting with the same parameters as in the NPT runs. Moreover, the corrections for energy and pressure has not been applied at this step of procedure. The values for the surface tension, γ, follow from the combination of the time averages for the components of the pressure tensor,

$$\gamma = \frac{1}{2}L_z\left\langle [P_{zz} - \frac{1}{2}(P_{xx} + P_{yy})]\right\rangle, \tag{3.4}$$

where P_{ij} are the components of the pressure tensor along i, j axes, and $\langle \ldots \rangle$ denotes the time average. We performed 9–10 consecutive runs at a constant volume, each piece with duration of 6 ns, and obtained the result for γ by averaging. The experimental results were taken from [67].

Principal feature of the simulation results is that all united atom models in question substantially overestimate the values for the surface tension of mixtures with dominating amount of DMSO species. Agreement with experimental data is qualitative rather than quantitative. For methanol-rich mixtures, the quality of results is much better. The reason of this behavior is that the alcohol model was parameterized with the surface tension as a target, apart from density and dielectric constant [27]. By contrast, the DMSO united atom models from literature were parameterized using the density and vaporization enthalpy as targets solely. The curves for $\gamma(X_\mathrm{D})$ from simulations seem to be almost linear. Therefore, the excess surface tension, $\Delta\gamma$, values are small. Insufficient accuracy of the DMSO models in this respect precludes capturing the deviation from ideality with reasonable precision. The best description of $\Delta\gamma(X_\mathrm{D})$ is provided by the P2–UAMI model.

4. Summary and conclusions

Principal objective of this computer simulation work was to explore mixing properties of a mixture composed of a polar aprotic solvent (DMSO) and alcohol species (amphiphilic molecules possessing both hydrophobic and hydrophilic groups). We restricted our attention to methanol as the simplest alcohol. Our study applies united atom models of these two species. Two models of methanol, TraPPE and UAMI, are used. On the other hand, several models for DMSO are considered. Namely, we use the P2, OPLS, VLL, VB, GOVG and Bordat et al. models, see table 1 in the models section. Motivation of this “low level” modelling is that the available knowledge of the properties of these systems from computer simulations is not comprehensive. Moreover, theoretical predictions have not been confronted and tested with respect to a quite wide available experimental data for various properties. The recently developed successful strategy for modelling the pure alcohols involved their density, the dielectric constant and surface tension as targets. In general terms, this approach permitted to describe the self-diffusion coefficient, shear viscosity, critical properties of pure alcohols and their solubility in water [68]. Applicability of this procedure to other systems and a wider set of properties has not been fully proven so far.

On the other hand, the present day parametrization of the DMSO united atom models involves the liquid density and vaporization enthalpy as targets, solely. In spite of much efforts, using modification of the parameters of inter-particle interactions and intra-molecular structure, the quality of results for several properties is not perfect. In order to attempt a better modelling, one should have clear vision of the problems necessary to solve for the description of DMSO-alcohol mixtures. We are aware of a more sophisticated modelling of DMSO (flexible all-atom, polarizable, ab initio) proposed in, e.g., [32, 33, 69]. However, much future work is necessary to systematically advance with this level of theory to applications.

In this work, we explored a wide set of properties for DMSO–MeOH mixtures. They include density and excess mixing density, molar volume and excess mixing volume, excess mixing enthalpy, average number of hydrogen bonds of similar and dissimilar species, dielectric constant, self-diffusion coefficients and shear viscosity, surface tension and excess surface tension. In all cases, we intended to critically evaluate the results versus experimental data. A few aspects of the microscopic structure are discussed as well. Unfortunately, the experimental counterpart, concerning the structural properties on composition, is missing. As concerns thermodynamic properties, such as self-diffusion coefficients, static dielectric constant, surface tension and shear viscosity, for practical use we would recommend the VLL, Bordat et al., GOVG models combined with UAMI methanol model. Indeed, they provide a quite reasonable agreement with experimental data for various properties. However, the accuracy of some excess properties from simulations of united atom models is not perfect. Nevertheless, application of a set of these DMSO models with UAMI methanol is recommended with necessary extensions, rather than to confide in the results from a single, distinguished model. Perhaps the findings of present work can be used to extend the training sets and incorporate them into the protocols of machine learning methods for studies of solubility of various compounds in DMSO as discussed in [70].

Apparently, there are two principal problems to be solved. One of them is in a better parametrization of pure DMSO considering different small sets of properties as targets, in the spirit of parametrization procedure proposed for alcohols and more complex molecules [68, 71]. The second one lies in elucidation and appropriate description of the cross interaction effects, i.e., of correlations between dissimilar species. It seems that inclusion of the structural aspects of mixing into targets would be beneficial. To implement this issue would require experimental studies via various diffraction techniques. Unfortunately, we are not aware of the activities along this line of research.

Having in mind that the entire set of properties for the systems under study follows from a balance of dipole-dipole interactions and association effects leading to hydrogen bonding, it would be profitable to perform additional calculations of the properties permitting interpretation of spectroscopic results, see, e.g., [72]. All these issues are under exploration in our laboratory at present.

Acknowledgements

O.P. acknowledges helpful discussions with Dr. Laszlo Pusztai concerning various aspects of experimental research and interpretation of data for systems of the present study. M.C.S. is grateful to Dr. Carlos Vega for illuminating discussions concerned with calculations of shear viscosity. We are grateful to Dr. Taras Patsahan for his interest to this work and his important comments concerning the improvement of the manuscript. We acknowledge a valuable technical support of this work by Magdalena Aguilar at Instituto de Quimica de la UNAM.

Appendix

Additional information for the composition dependence of self-diffusion coefficients.

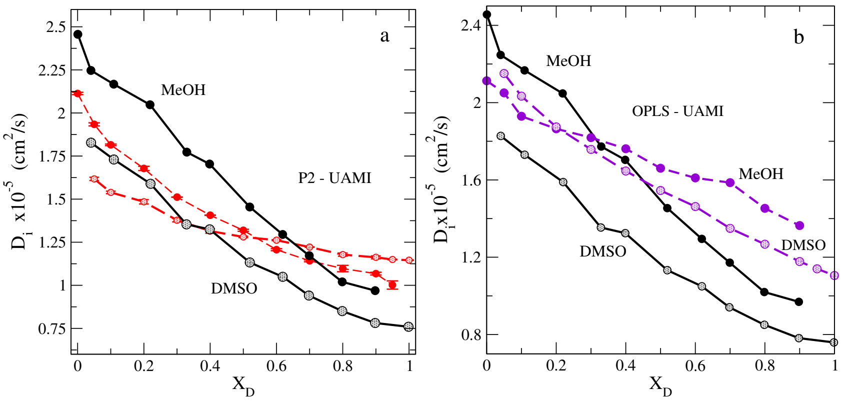

Figure A.1. (Colour online) The dependence of the self-diffusion coefficients of species on composition for DMSO–MeOH mixtures with P2–UAMI (panel a) and OPLS–UAMI (panel b) models. The experimental data are from [14].

Within these two models, one observes a crossover of the self-diffusion coefficients of MeOH and DMSO species, in contrast to experimental data see figure A.1.

References

1. Jacob S. W., Rosenbaum E. E., Wood D. C. (Eds.), Dimethyl sulfoxide, Marcel Dekker, New York, 1971.
2. Martin D., Weise A., Niclas H.-J., Angew. Chem. Int. Ed. Engl., 1967, **6**, No. 4, 318–334, doi:10.1002/anie.196703181.
3. Martin D., Hauthal H. G., Dimethyl Sulfoxide, Wiley, New York, 1975.
4. McGann L. E., Walterson M. L., Cryobiology, 1987, **24**, 11, doi:10.1016/0011-2240(87)90003-4.
5. Murthy S. S. N., J. Phys. Chem., 1997, **101**, 6043, doi:10.1021/jp970451e.
6. Ehrlich L. E., Feig J. S. G., Schiffres S. N., Malen J. A., Rabin Y., PLoS One, 2015, **10**, e0125862, doi:10.1371/journal.pone.0125862.
7. Markarian S. A., Asatryan A. M., Grigoryan K. R., Sargsyan H. R., Biopolymers, 2006, **82**, 1, doi:10.1002/bip.20454.
8. Yan Y., Zhang J., Chen L., Ren G., Zhou L., Liu L., Zhang X., Ouyang C., Wang H., Han J., J. Mol. Liq., 2024, **414**, 126204, doi:10.1016/j.molliq.2024.126204.
9. Bergman G., Leifer N., Zhigalenok Y., Malchik F., Sharon D., Aurbach D., Zhang Y., Goobes G., Shpigel N., ACS Appl. Mater. Interfaces, 2026, **18**, No. 6, 9750–9763, doi:10.1021/acsami.5c21318.
10. Xie P., Jin S., Sun C., Xie Y., J. Nanosci. Nanotechnol., 2020, **20**, 4799, doi:10.1166/jnn.2020.18482.
11. Wiewiór P. P., Shirota H., Castner E. W., Jr., J. Chem. Phys., 2002, **116**, 4643, doi:10.1063/1.1449864.
12. Noack K., Kiefer J., Leipertz A., ChemPhysChem, 2010, **11**, 630, doi:10.1002/cphc.200900691.
13. Ferris T. D., Zeidler M. D., Farrar T. C., Mol. Phys., 2000, **98**, 737, doi:10.1080/00268970009483343.
14. Virk A. S., Codling D. J., Stait-Gardner T., Price W. S., ChemPhysChem, 2015, **16**, 3814, doi:10.1002/cphc.201500670.
15. Chaban V. V., Andreeva N. A, J. Solution Chem., 2022, **51**, 788, doi:10.1007/s10953-022-01167-x.
16. Polyakov P., Wiegand S., J. Chem. Phys., 2008, **128**, 034505, doi:10.1063/1.2819672.
17. Rao B. G., Singh U. C., J. Amer. Chem. Soc., 1990, **112**, 3803, doi:10.1021/ja00166a014.
18. Chattoraj S., Chowdhury R., Ghosh S., Bhatttacharyya K., J. Chem. Phys., 2013, **138**, 214507, doi:10.1063/1.4808217.
19. Xin N., Sun Y., He M., Radke C. J., Prausnitz J. M., Fluid Phase Equil., 2018, **461**, 1, doi:10.1016/j.fluid.2017.12.034.
20. Santos N. C., Figueira-Coelho J., Martins-Silva J., Saldanha C., Biochem. Pharmacol., 2003, **65**, 1035, doi:10.1016/S0006-2952(03)00002-9.

21. Wen X., Zhang Z., Yue T., Zhang Q., Wang J., Zuo Y., J. Chem. Eng. Data, 2026, **71**, 2629, doi:10.1021/acs.jced.6c00130.
22. Long B., Ind. Eng. Chem. Res., 2011, **50**, 7019, doi:10.1021/ie102134g.
23. Semino R., Zaldivar G., Calvo E. J., Laria D., J. Chem. Phys., 2014, **141**, 214509, doi:10.1063/1.4902837.
24. Busch J., Ludwig R., Paschek D., J. Phys. Chem. B, 2025, **129**, 2573, doi:10.1021/acs.jpcb.4c08526.
25. Jorgensen W. L., J. Phys. Chem., 1986, **90**, 1276, doi:10.1021/j100398a015.
26. Chen B., Potoff J. J., Siepmann J. I., J. Phys. Chem. B, 2001, **105**, 3093, doi:10.1021/jp003882x.
27. García-Melgarejo V., Núñez-Rojas E., Alejandre J., J. Mol. Liq., 2021, **323**, 114576, doi:10.1016/j.molliq.2020.114576.
28. Gonzalez-Salgado D., Vega C., J. Chem. Phys., 2016, **145**, 034508, doi:10.1063/1.4958320.
29. Jorgensen W. L., Maxwell D., Tirado-Rives S., J. Am. Chem. Soc., 1996, **118**, 11225, doi:10.1021/ja9621760.
30. Chalaris M., Marinakis S., Dellis D., Fluid Phase Equilib., 2008, **267**, 47, doi:10.1016/j.fluid.2008.02.019.
31. Idrissi A., Marekha B., Jedlovszky P., J. Phys. Chem. B, 2014, **118**, 8724, doi:10.1021/jp503352f.
32. Strader M. L., Feller S. E., J. Phys. Chem. A, 2002, **106**, 1074, doi:10.1021/jp013658n.
33. Bachmann S. J., van Gunsteren W. F., J. Phys. Chem. B, 2014, **118**, 10175, doi:10.1021/jp5035695.
34. Bako I., Pusztai L., Pizio O., J. Chem. Phys., 2025, **163**, 194504, doi:10.1063/5.0300069.
35. Aguilar M., Pusztai L., Pizio O., Condens. Matter Phys., 2026, **29**, 13502, doi:10.5488/CMP.29.13502.
36. Aguilar M., Nuñez-Rojas E., Pizio O., Condens. Matt. Phys., 2026, **29**, 13503, doi:10.5488/CMP.29.13503.
37. Chang Ch.-K., Siepmann J. I., J. Chem. Eng. Data, 2024, **69**, 509, doi:10.1021/acs.jced.3c00415.
38. Geerke D. P., Oostenbrink C., van der Vegt N. F. A., van Gunsteren W. F., J. Phys. Chem. B, 2004, **108**, 1436, doi:10.1021/jp035034i.
39. Vechi S. M., Skaf M., J. Chem. Phys., 2005, **123**, 154507, doi:10.1063/1.2085052.
40. Luzar A., Chandler D., J. Chem. Phys., 1993, **98**, 8160, doi:10.1063/1.464521.
41. Zheng Y.-J., Ornstein R. L., J. Am. Chem. Soc., 1996, **118**, 4175, doi:10.1021/ja9539195.
42. Vaisman I. I., Berkowitz M. L., J. Am. Chem. Soc., 1992, **114**, 7889, doi:10.1021/ja00046a038.
43. Vishnyakov A., Lyubartsev A. P., Laaksonen A., J. Phys. Chem. A, 2001, **105**, 1702, doi:10.1021/jp0007336.
44. Bordat P., Sacristan J., Reith D., Girard S., Glattli A., Muller-Plathe F., Chem. Phys. Lett., 2003, **374**, 201, doi:10.1016/S0009-2614(03)00550-5.
45. Oostenbrink C., Villa A., Mark A. E., van Gunsteren W. F., J. Comput. Chem., 2004, **25**, 1656, doi:10.1002/jcc.20090.
46. Gujt J., Cazares Vargas E., Pusztai L., Pizio O., J. Mol. Liq., 2017, **228**, 71, doi:10.1016/j.molliq.2016.09.024.
47. Aguilar M., Dominguez H., Pizio O., Condens. Matter Phys., 2022, **25**, 33202, doi:10.5488/CMP.25.33202.
48. Spoel D., Lindahl E., Hess B., Groenhof B., Mark A. E., Berendsen H. J. C., J. Comput. Chem., 2005, **26**, 1701, doi:10.1002/jcc.20291.
49. Nikam P. S., Jadhav M. C., Hasan M., J. Chem. Eng. Data, 1996, **41**, 1028, doi:10.1021/je9600358.
50. Torres R. B., Marchiore A., Volpe P., J. Chem. Thermodyn., 2006, **38**, 526, doi:10.1016/j.jct.2005.07.012.
51. Kimura T., Morikuni T., Chanoki T., Takagi S., Netsu Sokutei, 1990, **17**, 67, doi:10.11311/jscta1974.17.67.
52. Galicia-Andrés E., Pusztai L., Temleitner L., Pizio O., J. Mol. Liq., 2015, **209**, 586, doi:10.1016/j.molliq.2015.06.045.
53. Méndez-Bermudez J. G., Dominguez H., Temleitner L., Pusztai L., Phys. Status Solidi B, 2018, **255**, 180025, doi:10.1002/pssb.201800215.
54. Kumar R., Schmidt J. R., Skinner J. L., J. Chem. Phys., 2007, **126**, 204107, doi:10.1063/1.2742385.
55. Zhang N., Li W., Chen C., Zuo J., Weng L., Mol. Phys., 2013, **111**, 939, doi:10.1080/00268976.2012.760050.
56. Galicia-Andrés E., Dominguez H., Pusztai L., Pizio O., J. Mol. Liq., 2015, **212**, 70, doi:10.1016/j.molliq.2015.08.061.
57. Li Q., Wu G., Yu Z., J. Am. Chem. Soc., 2006, **128**, 1438, doi:10.1021/ja0569149.
58. Neumann M., Mol. Phys., 1983, **50**, 841, doi:10.1080/00268978300102721.
59. Romanowski S. J., Kinart C. M., Kinart W. J., J. Chem. Soc. Faraday Trans., 1995, **91**, 65, doi:10.1039/FT9959100065.
60. Guo-Zhu J., Jie Q., Fluid Phase Equilib., 2014, **365**, 5, doi:10.1016/j.fluid.2013.12.014.
61. Luzar A., J. Mol. Liq., 1990, **46**, 221, doi:10.1016/0167-7322(90)80056-P.
62. Baluja S., J. Anal. Pharm. Res., 2021, **10**, 169, doi:10.15406/JAPLR.2021.10.00383.
63. González M. A., Abascal J. L. F., J. Chem. Phys., 2010, **132**, 096101, doi:10.1063/1.3330544.
64. Kumar S., Sarkar S., Bagchi B., J. Chem. Phys., 2019, **151**, 194505, doi:10.1063/1.5126381.
65. Fischer N. M., van Maaren P. J., Ditz J. C., Yildirim A., van der Spoel D., J. Chem. Theory Comput., 2015, **11**, 2938, doi:10.1021/acs.jctc.5b00190.
66. Zubillaga R. A., Labastida A., Cruz B., Martinez J. C., Sanchez E., Alejandre J., J. Chem. Theory Comput., 2013, **9**, 1611, doi:10.1021/ct300976t.

67. Bagheri A., Fazli M., Bakshaei M., J. Chem. Thermodyn., 2016, **101**, 236, doi:10.1016/j.jct.2016.06.004.
68. Salas F. J., Méndez-Maldonado G. A., Núñez-Rojas E., Aguilar-Pineda G. E., Dominguez H., Alejandre J., J. Chem. Theory Comput., 2015, **11**, 683, doi:10.1021/ct500853q.
69. Mancini L., Lombardi A., Pirani F., Pacifici L., Rosi M., Faginas-Lago N., In: Computational Science and Its Applications – ICCSA 2024 Workshops, Vol. 14823, Gervasi O., Murgante B., Garau C., Taniar D., C. Rocha A. M. A., Faginas Lago M. N. (Eds.), Springer Nature Switzerland, Cham, 2024, 361–374, doi:10.1007/978-3-031-65329-2_24.
70. Tetko I. V., Novotarskyi S., Sushko I., Ivanov V., Petrenko A. E., Dieden R., Lebon F., Mathieu B., J. Chem. Inf. Model., 2013, **53**, No. 8, 1990–2000, doi:10.1021/ci400213d.
71. Salas F. J., Núñez-Rojas E., Alejandre J., J. Mol. Liq., 2025, **427**, 127467, doi:10.1016/j.molliq.2025.127467.
72. Bone R., Schwarz K., J. Chem. Phys., 2026, **164**, 094502, doi:10.1063/5.0320783.

Моделювання рідких сумішей ДМСО–МеОН методом молекулярної динаміки. Вплив силових полів на властивості змішування

М. Крус-Санчес [1], О. Пізіо [2]

[1] Хімічний факультет Автономного університету Метрополітана-Істапалапа, просп. Сан Рафаель Атлікско 186, кол. Віцентіна, 09340, CDMX, Мехіко, Мексика

[2] Інститут хімії, Національний Автономний університет Мехіко, Сіркіто Екстеріор, 04510, Мехіко, Мексика

За допомогою комп'ютерного моделювання молекулярної динаміки вивчається залежність основних властивостей рідких сумішей диметилсульфоксиду (ДМСО)-метанолу (МеОН) від їх складу. Досліджено набір неполяризовуваних напівгнучких моделей для молекули ДМСО в поєднанні з моделями метанолу. Оцінено тенденції зміни складу густини, надлишкового об'єму змішування та надлишкової ентальпії змішування. Окрім того, вивчається залежність самодифузії частинок, зсувної в'язкості, статичної діелектричної проникності та поверхневого натягу від складу суміші. Проаналізовано певні аспекти мікроскопічної структури з точки зору радіальних функцій розподілу та середньої кількості молекул з водневими зв'язками. Якість багатьох комбінацій моделей проілюстровано та критично оцінено шляхом порівняння з експериментальними даними.

Ключові слова: *молекулярна динаміка, метанол, диметилсульфоксид, густина, діелектрична проникність, поверхневий натяг, коефіцієнти самодифузії, зсувна в'язкість*